HHS Public Access

Author manuscript

Biomaterials. Author manuscript; available in PMC 2017 April 01.

Published in final edited form as:

Biomaterials. 2016 April ; 84: 86–98. doi:10.1016/j.biomaterials.2015.11.032.

Structure-Property Relationship for *in Vitro* siRNA Delivery Performance of Cationic 2-Hydroxypropyl-β-cyclodextrin: PEG-PPG-PEG Polyrotaxane Vectors

Vivek D. Badwaik[1], **Emilio Aicart**[1,2], **Yawo A. Mondjinou**[1], **Merrell A. Johnson**[3], **Valorie D. Bowman**[4], and **David H. Thompson**[1,*]

[1]Department of Chemistry, Multi-disciplinary Cancer Research Facility, Bindley Bioscience Center, 1203 W. State Street, West Lafayette, IN, 47907, USA

Abstract

Nanoparticle-mediated siRNA delivery is a promising therapeutic approach, however, yet the processes required for transport of these materials across the numerous extracellular and intracellular barriers are poorly understood. Efficient delivery of siRNA-containing nanoparticles would ultimately benefit from an improved understanding of how parameters associated with these barriers relate to the physicochemical properties of the nanoparticle vectors. We report the synthesis of three Pluronic®-based, cholesterol end-capped cationic polyrotaxanes (PR^+) threaded with 2-hydroxypropyl-β-cyclodextrin (HPβCD) for siRNA delivery. The biological data showed that PR^+:siRNA complexes were well tolerated (~90% cell viability) and produced efficient silencing (>80%) in HeLa-GFP and NIH 3T3-GFP cell lines. We further used a multi-parametric approach to identify relationships between the PR^+ structure, PR^+:siRNA complex physical properties, and biological activity. Small angle x-ray scattering and cryoelectron microscopy studies reveal periodicity and lamellar architectures for PR^+:siRNA complexes, whereas the biological assays, ζ potential measurements, and imaging studies suggest that silencing efficiency is influenced by the effective charge ratio (ρ_{eff}), polypropylene oxide (PO) block length, and central PO block coverage (i.e., rigidity) of the PR^+ core. We infer from our findings that more

[*]**Corresponding Author.** David H. Thompson, Tel: 765-494-0386; davethom@purdue.edu.

[2]**Present Addresses.**

Grupo de Química Coloidal y Supramolecular, Departamento de Química Fisica I, Facultad de Ciencias Quimicas, Universidad Complutense de Madrid, 28040-Madrid, Spain

[3]Department of Physics, Indiana University-Purdue University Indianapolis, Indiana 46202, USA

[4]Discovery Park, Hockmeyer Hall of Structural Biology, Purdue University, West Lafayette, Indiana 47907, USA

Supporting Information Available. Further characterisation and methods (values of q_{100}, d_{100}, q_{siRNA}, and d_{siRNA} of the lamellar ($L\alpha$) structures, particle diameters by DLS, gel shift assay of F127-, L35- and L81-based PR^+:siRNA complexes, MTS cell viability assay for NIH 3T3-GFP cells, Raw flow cytometry data for transfection of HeLa-GFP cells, two-color flow cytometry analysis of GFP silencing in HeLa-GFP cells, confocal microscopy of HeLa-GFP cells, with and without L81-PR^+:siRNA complexes). This material is available free of charge via the Internet at http://www.journals.elsevier.com/biomaterials/

Author Contributions

The manuscript was written through contributions of all authors. All authors have given approval to the final version of the manuscript.

Conflict of Interest: The authors declare no competing financial interest.

compact PR^+:siRNA nanostructures arising from lower molecular weight, rigid rod-like PR^+ polymer cores produce improved silencing efficiency relative to higher molecular weight, more flexible PR^+ vectors of similar effective charge. This study demonstrates that PR^+:siRNA complex formulations can be produced having higher performance than Lipofectamine® 2000, while maintaining good cell viability and siRNA sequence protection in cell culture.

Keywords

gene silencing; siRNA; polyrotaxane; β-cyclodextrin; cryoelectron microscopy; small angle x-ray scattering

INTRODUCTION

Post-transcriptional gene silencing by RNA interference (RNAi) represents a promising new approach for the targeted inhibition of gene expression. Potential new therapeutic applications have been rapidly developing due to the small 21–29 nucleotide sequence lengths needed to elicit an RNAi response and the attractive opportunities that exist in treating cancer, neurological disorders, and cardiovascular diseases with this approach [1, 2]. Unfortunately, the impact of this therapeutic modality has been limited by the absence of clinically validated synthetic delivery vehicles that are highly efficient and display low toxicity. Viral vectors, although efficient and persistent, are challenged by issues such as large-scale production, immunogenicity, and safety. Non-viral vectors are limited primarily by low efficiency, however commercial scalability and low host immunogenicity relative to viral vectors has maintained interest in further development of this approach [3]. Many different non-viral delivery vehicles have been explored for siRNA delivery, including nanoparticle complexes based on cationic lipids [4], cyclodextrin oligomers [5], lipid/Ca^{2+} mixtures [6], Au [7] or PLGA nanoparticles [8], and many other nanoparticle platforms [9]. All of these nanoparticle vehicles are capable of protecting the nucleic acid from enzymatic degradation and enhancing the cell permeability of the siRNA cargo to boost siRNA delivery into target cells; however, most of these vehicles possess unwanted toxicity, serum instability, and/or unfavorable immunogenicity profiles [10, 11]. Moreover, transition of these compounds from *in vitro* to *in vivo* studies has been an unmet challenge that may be attributed to an inadequate knowledge of the structure-activity relationships governing the performance of non-viral complexes [12, 13]. Consequently, the results of *in vitro* experiments often cannot be directly translated or extrapolated to the *in vivo* process. This limitation underscores the need for more extensive physicochemical and biological studies to improve our understanding of polyplex structure and the transfection process for subsequent *in vivo* applications [14].

Supramolecular structures such as polyrotaxanes (PR) are a new class of vectors that have been explored for the transfection applications. PR structures consist of polymers ‘axle’ that is threaded through macrocyclic molecules ‘wheels’ and is endcapped with bulky groups that prevent dethreading. In previous reports, cationic cyclodextrin (CD) PR^+s have been evaluated for their DNA complexation and *in vitro* transfection ability, where macrocyle were first threaded onto the polymer backbone followed by introduction of cationic

substituents by post-modification reactions [15]. The first generation of PR consisted of a central PEG scaffold that was threaded through cationic α-CDs and the scaffold was terminated in disulfide bonds, providing degradability within the reducing environment of the cell [16–18]. Receptor specific PR^+, with targeting ligands on the endcap have also been synthesized to promote uptake within the cell [19]. A temperature-activated threading of CDs onto water soluble ionenes was recently demonstrated for the formation of PR and was used for delivery of pDNA and siRNA [20]. This technique showed formation of more structurally well-defined PR^+ which were easier to synthesize as it excludes the random post-modification step of the earlier PR. In previous studies our group has demonstrated the potential of linear and branched cationic α-CD PR^+ as efficient siRNA delivery vehicles [21, 22]. Recently Yui group has developed the PEG based PR^+ with α-CDs for siRNA delivery and shown that more highly threaded PR^+ are more effective siRNA delivery agents [23]. By varying the number of threading CDs and Dimethylethanolamine (DMAE) groups on the PR, they established a relationship between charge density and threading efficiency on the performance of DMAE-PR^+/siRNA polyplexes. They have concluded that PRs with larger numbers of threaded CDs exhibited higher siRNA binding abilities than flexible PRs [23–25].

In this report, we describe the synthesis, biophysical characterization, and biological performance of structurally related series of cationic polyrotaxanes (PR^+), comprised of Pluronic® block copolymers threaded within *N*,*N*-dimethylaminoethylamine (DMEDA)-modified 2-hydroxypropyl-β-cyclodextrin (HPβCD) macrocycles and end-capped with cholesterol, as potentially efficient and low toxicity siRNA delivery vehicles [26, 27] (Figure 1).

Zeta (ζ) potential measurements were performed to determine the effective charge of each cationic PR^+ compound ($q_{eff\ PR+}$) as well as the electroneutrality ratio $(m_{PR}+/m_{RNA})\varphi$ of each polyplex (i.e., the point where the PR^+ positive charges and the siRNA negative charges balance at $\rho_{eff} = 1$). Cryogenic transmission electron microscopy (cryo-TEM), dynamic light scattering (DLS), and small-angle X-ray scattering (SAXS) methods were also employed to reveal the size, morphology, and supramolecular structure of the PR^+:siRNA complexes. Finally, we have evaluated the biological performance of the complexes using flow cytometry and confocal fluorescence microscopy to monitor cellular localization, cell viability/cytotoxicity, and GFP knockdown efficiency of the three PR^+: siRNA complex.

Our findings show that PR^+:siRNA complexes form lamellar structures. We also observe that the size, rigidity, and effective charge ratios, ρ_{eff}, of the PR^+ and its complexes play a key role in determining the silencing efficiency. These findings establish a structure-biological activity relationship that can be used for future materials designs and to provide insights into the mechanism of siRNA complexation and release after internalization to elicit an RNAi response. It also provides important information for the production of optimal polyplex formulations that can afford good siRNA protection, while employing a minimum amount of PR^+ vector, for subsequent biomedical applications that require low toxicity and high efficiency transfection complexes.

MATERIALS AND METHODS

Materials for PR$^+$ Synthesis

Triblock copolymers Pluronic® F127 (EO 200, PO 65), L35 (EO 22, PO 16), and L81 (EO 6, PO 43) were purchased form Sigma-Aldrich (USA) in powder form and dried by azeotropic distillation from benzene before use. Other reagents such as *N*,*N*-dimethylethylenediamine (DMEDA), 2-Hydroxypropyl-β-cyclodextrin (with average degree of hydroxypropyl substitution = 6.8), triethylamine (TEA), tris(2-aminoethyl)amine (TAEA), cholesteryl chloroformate, and carbonyldiimidazole (CDI), were also purchased from Sigma-Aldrich (USA) and used without further processing. Except DCM and DMF, all the solvents were used without further purification; DMF and DCM were dried over CaH_2, filtered, distilled at low pressure and stored under Ar environment prior to use. Cellulose dialysis membranes (Spectrum Labs, USA) were rinsed thrice followed by immersion in deionized water for at least 30 min at room temperature prior to use. Ultra-pure H_2O (resistivity ≈ 18.0 MΩ/cm^{-1}) was used for all the experiments and was obtained from a NANOpure water purification system.

Materials for Transfection Complex Formulation and Biological Assays

GFP-22 siRNA was purchased from Qiagen (USA) and scrambled siRNA (custom 22 mer) was purchased from GE Healthcare Dharmacon (USA) (Sense Strand: 5'- GCA AGC TGA CCC TGA AGT TC (dTdT)-3', anti-sense strand 3'- GAA CUU CAG GGU CAG CUU GC-5', Mol. Wt. 13,965.6 (g/mol), the oligonucleotide has been converted to the 2'-hydroxyl, and annealed), Inc. MTS reagent was purchased from Promega (USA). Lipofectamine® 2000 (L2K) transfection reagent, SYTOX® Red dead cell stain, LysoTracker® Blue DND-22, and AlexaFluor®680 Wheat Germ Agglutinin- (AlexaFluor® 680 WGA) conjugate were purchased from Life Technologies (USA). Label IT® siRNA Tracker intracellular localization kit (Cy3) was obtained from Mirus (USA). Fetal Bovine Serum (FBS), DMEM and RPMI media, sodium pyruvate, PBS and trypsin, were purchased from Atlanta Biologicals (USA). Mark-tubes made of borosilicate glass #50, (L= 80 OD= 1.50 Wall= 0.01 mm) were purchased from Hilgenberg GmbH (Germany).

Synthesis of DMEDA-HPβCD:Pluronic-Chl Polyrotaxanes (PR$^+$)

The PR$^+$ (Figure 1, Table 1) were synthesized using a previously reported protocol [27, 28].

Formulation of PR$^+$:siRNA Complexes

We optimized the condition for L2K in HeLa-GFP and NIH 3T3-GFP using the suggested protocol by the vendor (Life Technologies, USA) with a few modifications to achieve maximum silencing efficiency with moderate toxicity (cell viability >95%) in our cell lines. Based on these observations, we found that 100 nmol of siRNA was enough to provide maximum effect for a given population of cells; this quantity was then kept constant for the polyrotaxane-based complexes.

The nanoplexes were formulated in 20 mM HEPES, pH 7.4 buffer and for all biological studies, a final siRNA concentration of 100 nM was used, similar to that recommended for the benchmark positive control, L2K.

For typical a polyplex formation, siRNA solution (either GFP-22 siRNA, scrambled siRNA, or Cy3-labeled GFP-22 siRNA (siRNA-Cy3)) was vortex mixed with a PR^+ solution (2 – 10 μg/mL, depending on ρ_{eff}) in HEPES buffer. The ρ_{eff} ratios were varied between 0 and 15 to identify the optimum concentration of PR^+ required to provide both high colloidal stability and good biological performance.

Characterization of Polyrotaxane-siRNA Polyplexes

ζPotential and Particle Size Analysis—The electrophoretic mobility, particle size, and size distribution of PR^+:siRNA complexes were determined by dynamic light scattering using a particle size analyzer (Zetasizer Nano S, Malvern Instruments) at 20 °C with a scattering angle of 90°. Each electrophoretic mobility value reported was an average over 30 independent measurements. ζ potentials were obtained from the measured electrophoretic mobility, using the Henry equation. siRNA complexes (20 μg in 50 μL of HEPES) of increasing PR^+ content ($m_{PR}+/ m_{RNA}$) were formulated and incubated at 4 °C for 1 h. After incubation, all complexes were diluted to 1 mL by HEPES buffer and measured using a Zetasizer Nano-S, (Malvern Instruments Ltd.) at a scattering angle of 90°. At least 40 measurements were made and averaged for each sample for ζ-potential determination

Cryo-Transmission Electron Microscopy (cryo-TEM)—Cryo-TEM experiments were conducted following the general procedures reported previously [29, 30], except that Quantifoil R1.2/1.3 (1.2 mm hole diameter) on 400-mesh copper grids were used as sample substrates. Images were obtained using a Titan Krios cryo-electron microscope operating at 300 kV under low-dose conditions at a nominal magnification of 29,000× and using different degrees of defocus (-3 to-10 nm) to obtain adequate phase contrast. Images were recorded using an Ultra Scan 4000 Gatan digital camera. These Charge-coupled device (CCD) images were processed and analyzed (Gatan, Inc). Experiments were carried out for PR^+:siRNA complexes at effective charge ratios (ρ_{eff}) of 2 and 3. For the TEM analysis all the complexes were made at high pDNA concentration (60 μg/50 μL) in HEPES buffer and analysed. Samples for SAXS (80 μg/μL) were made in small cpillaries tube and the samples were dried in hot oven at 40 °C so as to evaporate excess water. Small-angle X-ray scattering (SAXS) experiments were carried out utilizing a NanoStar SAXS system (Bruker, Germany). An incident beam, fixed at ~8 keV, was employed, with a 0.4 mm pinhole setup using a sample to detector distance of ≈ 26 cm. An HiStar xenon gas area detector (1024 × 1024 pixels) with a photon count ~ 1500 photons/second was used for data collection. Samples were placed in sealed glass capillaries (1.5 mm O.D. and 1.48 mm I.D.).

Small Angle X-ray Scattering (SAXS)—Small-angle X-ray scattering (SAXS) experiments were carried out utilizing a NanoStar SAXS system (Bruker, Germany). An incident beam, fixed at ~8 keV, was employed, with a 0.4 mm pinhole setup using a sample to detector distance of ≈ 26 cm. An HiStar xenon gas area detector (1024 × 1024 pixels) with a photon count ~ 1500 photons/second was used for data collection. Samples were placed in sealed glass capillaries (1.5 mm O.D. and 1.48 mm I.D.). Experiments were carried out at several effective charge ratios (ρ_{eff}) of the PR^+:siRNA complexes.

Gel Retardation Assay—The complexation behavior of PR^+ with siRNA was analyzed by gel retardation assay (4% agarose gel electrophoresis). The agarose gels were made in TBE electrophoresis buffer (pH 8.0) containing GelRed fluorescent stain at 1:10,000 dilution. PR^+:siRNA complexes with 0.2 μg of siRNA at different ρ_{eff} ratios were loaded in different wells onto the gel. All the samples were mixed with gel loading dye (1:5 dilution) before loading into the wells and electrophoresis was carried out at room temperature and at constant voltage of 55 V for 90 min in TBE electrophoresis buffer. The GFP22-siRNA bands were then analyzed using FluorChem E System at a wavelength of 365 nm.

Biological Performance

Cell Viability Assay—Cytotoxicity profile of all the PR^+:siRNA complexes relative to L2K and untreated cells was evaluated using the MTS assay in a human cervical cancer cell line (HeLa-GFP) and a murine fibroblast cell line (NIH 3T3-GFP). Cell viabilities were measured as a function of increasing ρ_{eff}. The cells at densities of 10,000 cell/well were seeded in 96-well microtiter plates (Greiner, 96-well multiwall plates-fat bottom) in complete DMEM medium supplemented with 10% FBS at 37 °C, 5% CO_2, and 95% relative humidity. After 24 h (cell confluency of 80–90%), the culture media was replaced with serum-free media containing complexes with increasing ρ_{eff} and the cells were further incubated for 24 h. After 24h, MTS reagent (15μL) was added to each well and incubated for 2 h prior to readout. The absorbance was measured at a wavelength of 492 nm using a multimode plate reader (Beckman Coulter, DTX880). The blank correction was performed by subtracting the absorbance of the sample well just before addition of the MTS reagent. The cell viability (%) relative to control cells (untreated cells) was calculated as $[A]_{test}/[A]_{control} \times 100\%$, where $[A]_{control}$ is the absorbance of the control wells and $[A]_{test}$ is the absorbance of the wells with PR^+:siRNA. All samples were made in triplicates and cytotoxicity values reported are averaged from the three measurements.

Cellular Uptake Studies—Localization of the complexes within HeLa-GFP cells was studied by plating 100,000 cells per well at 37 °C, 5% CO_2, and 95% relative humidity in 24-well plates and incubating them for 24 h so as to reach cell confluency of 80–90% before the experiment. Complexes of siRNA-Cy3 with the PR^+ at different ρ_{eff} ratios were incubated with cells for 4 h at 37 °C in serum free media. After 4 h, the excess or non-cell associated particles were removed by aspirating the spent media and the cells were washed with PBS (3×), trypsinized, transferred to flow sample cells and then analyzed by flow cytometry (Beckman-Coulter FC500) using the FL3 channel.

In Vitro knockdown/Cell Viability Experiments—HeLa-GFP and NIH 3T3-GFP cells were cultured in complete DMEM medium as described for the uptake studies. After 24 h (cell confluency of 80–90%), the culture media was replaced with serum free media containing 90 pmol GFP22-siRNA complexes with PR^+ at ρ_{eff} ratios of 0.5–15. The cells were incubated with the complexes for 4 h, after which cells were washed three times with PBS, followed by addition of fresh serum-supplemented media. After total of 36 h incubation, the media was aspirated and the cells were washed with PBS (3×), detached form the surface using trypsin and collected in FACS analysis tubes. SYTOX® Red dead cell stain (1 μL) was added to each sample and incubated for 15 min before analysis by

FACS using the FL1 channel for GFP fluorescence and the FL4 channel for the fluorescence from SYTOX® stain. %GFP-positive cells, % GFP median fluorescence intensity, and % median intensity due to SYTOX® stain was collected and analyzed using FlowJo-v10 software relative to L2K. Statistical analysis for the biological studies was conducted by using R software (http://cran.r-project.org). Data are reported as absolute values or relatives to the controls. Normality was evaluated for each variable using Shapiro-Wilk test. Data with normal distribution were compared using ANOVA, and Bonferroni was used as post-hoc analysis.

Intracellular Trafficking of PR^+:siRNA Complexes—Temporal and spatial tracking of PR^+: siRNA was studied using the multiphoton confocal microscopy. The lysosomal compartments in the cytoplasm were stained using LysoTracker® Blue DND-22 while the plasma membrane was stained using AlexaFluor® 680 WGA. The GFP22-siRNA used in this study was tagged with Cy3 dye using a kit from Mirus, which attached of the label to siRNA without altering siRNA structure or affecting downstream target knockdown performance. HeLa-GFP cells were cultured in complete DMEM medium supplemented with 10% FBS at a cell density of 35,000 cells/well in 4 chambered glass slides. After 24 h, the culture media was replaced with DMEM media containing the PR^+:siRNA-Cy3 complexes at an ρ_{eff} ratio of 3. The cells were incubated with the complexes for various time points (2, 4, 9, 24, 36 and 48 h) after which they were stained with AlexaFluor® 680 WGA (5 μL) for 10 min, washed with PBS (2×), and followed by incubation with 2 μL LysoTracker® Blue DND-22 for 10 min. The cells were then washed with PBS (3×) and observed under a confocal microscope (Nikon A1R MP) using a 60× silicone oil objective.

RESULTS AND DISCUSSION

PR^+:siRNA Electrostatic Interactions

Effective non-viral nucleic acid delivery requires knowledge of the electroneutrality characteristics of the transfection complexes being employed, since the complexes benefit form a net positive charge ($\rho_{eff} > 1$) to promote their interactions with the negative charges present on the plasma membrane of target cells. In addition, the effective charge ratio of the complex determines the structure, physical properties and biological response to the nucleic acid vector. We used, the total PR^+ vector to siRNA mass ratio ($m_{PR}+/m_{RNA}$) and the effective charge ratio (ρ_{eff}) between the positive PR^+ charges and the negative siRNA phosphate groups to define the polyplex composition. These quantities are related by the following equation:

$$\rho_{eff}=\frac{n^+}{n^-}=\frac{q_{eff\ PR^+}(m_{PR^+}/M_{PR^+})}{q_{eff\ RNA}(m_{RNA}/M_{RNA})}=\frac{q_{eff\ PR^+}M_{RNA}}{q_{eff\ RNA}M_{PR^+}}\left(\frac{m_{PR^+}}{m_{RNA}}\right) \quad (1)$$

where M_{PR+} and M_{RNA} are the molar masses of PR^+ and siRNA, respectively; n^+ and n^- are the number of moles of charges on the positive PR^+ and negative siRNA; and $q_{eff\ PR^+}$ and $q_{eff\ RNA}$ are the effective charges of $PR^+$and siRNA, respectively. Because an efficient cell transfection event is favored by complexes with a net positive charge, there is a specific electroneutrality ratio ($m_{PR}+/ m_{RNA}$) where $\rho_{eff} = 1$, that suggests a lower limit from which

the polyplex becomes a potentially efficient nucleic acid delivery vector [31]. Since this parameter is related to the potential and net charge of the transfection complex, zeta potential (ζ) measurements are the most widely used method for determining the electroneutrality mass ratio of the nanoparticle formulation, although other methods such as agarose gel electrophoresis and dye intercalation assays may also be used [32–35]. Figure 2 shows plots of ζ versus (m_{PR+}/m_{RNA}) for the three PR^+:siRNA complexes derived from L35-PR^+, L81-PR^+, and F127-PR^+. The electroneutrality ratio ($m_{PR}+/ m_{RNA}$)φ of the PR^+:siRNA transfection complexes is defined as the point where a sign inversion occurs in the sigmoidal ζ versus ($m_{PR}+/ m_{RNA}$) profile. This value, where $\rho_{eff} = 1$, is related to the previous quantities of Eq. 1 by

$$\left(\frac{m_{PR+}}{m_{RNA}}\right)_{\phi} = \frac{q_{eff\ RNA} M_{PR+}}{q_{eff\ PR+} M_{RNA}} \quad (2)$$

Many studies have shown that multivalent cationic gene vectors typically have an effective charge that is significantly lower than the nominal charge [31, 32, 36]. Therefore, determination of the effective charge is crucial for understanding the role of polyplex charge on transfection efficiency. Long linear DNA molecules (e.g., those containing thousands of base pairs like calf thymus DNA or salmon sperm DNA) and shorter DNA or RNA molecules (i.e., those containing 20–24 bp) have an effective negative charge ($q_{eff\ RNA}$) that matches its nominal charge (i.e., −2 per bp)[31, 37, 38]. Thus, the effective charge of any multivalent cationic transfection agent like the PR^+ used for siRNA complexation in this work ($q_{eff\ PR^+}$) can be determined from Eq. 2 (Table S2) using the experimentally determined electroneutrality mass ratio ($m_{PR}+/ m_{RNA}$)φ [31]. The obtained $q_{eff\ PR^+}$ values (Table 1) showed that the three cationic polyrotaxanes have a lower effective charge than its nominal one, ranging from 80%, 58% and 41% for L35-PR^+, L81-PR^+, and F127-PR^+, respectively.

This trend is not related to the number of HPβCD threaded onto the Pluronic® core, nor its nominal charges, effective charges, or molecular weight, but rather to the length and apparent rigidity of the highly threaded PO “axle” within the PR^+ core. We infer from these findings that as the polymer “axle” where the charged HPβCDs are threaded becomes longer and more flexible, the capability of their charged regions to fully interact with siRNA decreases, resulting in a lower percentage of effective charge.

Once the effective charge of each polyrotaxane ($q_{eff\ PR+}$) was determined, the effective charge ratio, ρ_{eff}, between the positive PR^+ and negative siRNA was also calculated using Eq. 1. The ρ_{eff} quantity is the key parameter enabling the preparation and characterization of polyplex for optimal silencing efficiency and minimal cytotoxicity due to lower net positive charge. It should also be noted that the ζ versus ($m_{PR}+/ m_{RNA}$) plots (Figure 2) reveal that the electroneutrality curves for each PR^+:siRNA has a different slope, such that the complexes formed by L81-PR^+ showed the steepest slope relative to L35- and F127-based PR^+:siRNA complexes. These trends are directly proportional to the effective charge on the polymer. The slope of the curve is likely correlated with the strength and stability of the PR^+:siRNA complexation, suggesting that the order of complex stability should be L81-

PR^+:siRNA > L35-PR^+:siRNA > F127-PR^+:siRNA. These findings are supported by cryo-TEM and agarose gel studies as described below.

Size, Structure, Morphology, and Stability of the PR^+:siRNA Transfection Complexes

The size, morphology, and structure of transfection complexes formed by non-viral vectors and DNA or RNA are well-known factors that impact their transfection and silencing efficiency [32, 38–43]. We analyzed these characteristics as a function of PR^+ type using DLS, gel electrophoresis, cryo-TEM, and SAXS techniques at several charge ratios in the useful range for gene silencing (ρ_{eff}>1). Initially, the size of the PR^+:siRNA complexes was determined by DLS. Average hydrodynamic diameters of 250 ± 25, 300 ± 20, and 300 ± 100 nm were obtained for the L81-PR^+:siRNA, L35-PR^+:siRNA, and F127-PR^+:siRNA complexes, respectively (Figure S1 & S2), at several effective charge ratios (ρ_{eff} > 1). We infer from these results that the size of the polyplex roughly correlates with the PR^+:siRNA complexation strength as indicated by the electrophoretic mobility analysis in Figure S-3. PR^+:siRNA stability analysis using gel shift analysis displayed that the complexation ability of PR^+ with siRNA increased with increasing ρ_{eff} ratio for all PR^+ species. It is noteworthy to compare the complexation behaviour among the PR^+ members, where F127 showed significant complexation (i.e., maximum amount of siRNA retained in the sample wells) above ρ_{eff} = 10, whereas a similar trend was observed for L35 and L81 at lower effective charges of ρ_{eff} >7.5 and ρ_{eff}> 5, respectively (Figure S-3)

Next, cryo-TEM images were collected for positively charged PR^+:siRNA complexes (ρ_{eff} > 1). Unfortunately, due to poor solubility and the low overall charge of F127-PR^+, it was not possible to prepare and analyze highly concentrated samples of this vector, or its siRNA complexes, for cryo-TEM and SAXS experiments. The micrographs shown in Figure 3A show typical nanoparticles formed by L81-PR^+: siRNA and L35-PR^+: siRNA complexation. From the analysis of these images, it can be concluded that they consist mostly of spherical nano-aggregates, with average diameters around 200 ±10 nm, in reasonable agreement with those found by DLS. Many of the complexes in Figure 3A show a roughly multilamellar arrangement, comprised of periodic monolayers that display a typical fingerprint-type pattern in their structure. Fast Fourier Transform (FFT) analysis of selected nano-aggregate particles as a probe for periodicity show a profile wherein the diffraction spots correspond to a lamellar pattern (Figure 3A, insets).

Interlamellar spacing averages of 7.6 ± 0.6 nm, and 7.4 ± 0.7 nm were obtained for L81-PR^+:siRNA and L35-PR^+:siRNA, respectively, consistent with the multilamellar structural features that have previously been reported for lipoplexes comprised of cationic lipids and plasmid DNA [32, 38] or siRNA [44] We conclude from these findings that the interlamellar spacing is a roughly constant value of 7.5 nm for all the PR^+:siRNA complexes in this study, since the same DMEDA-modified HPβCD “wheels” are threaded onto the Pluronic® “axle”, thereby yielding the same lamellar thicknesses for the three PR^+:siRNA transfection complexes. Thus, assuming a PR^+ thickness similar to that of the FIPβCD-$DMEDA^+$ diameter (4.8 nm), the remaining thickness of ~2.7 nm is sufficient to accommodate a monolayer of double-stranded siRNA. This multilamellar pattern is a frequently reported structure for lipoplexes,[31, 32, 44] with similar average values described for the

interlamellar distances of those assemblies, suggesting that there is no appreciable structural difference in siRNA compaction among cationic lipid vectors and these PR^+ constructs.

The cationic PR^+:siRNA complex structures were also investigated across a range of charge ratios ($\rho_{eff} > 1$) by SAXS. Figure 3B shows several SAXS diffractograms, plotted as intensity versus q factor. Bragg peaks apparent in these diffractograms show that the PR^+:siRNA complexes form a lamellar structure (L_α) with an interlayer distance (d) related to q of the first peak ($d = 2\pi/q_{100}$) (Table S-1). Thus, the PR^+:siRNA complexes may be represented as alternating layers of PR^+ and siRNA helixes, where $d(= d_m + d_w)$ is the sum of the monolayer thicknesses of the PR^+ (d_m) and siRNA (d_w) layers. The obtained d values are 8.0 ± 0.2 nm, and 8.1 ±0.2 nm for L81-PR^+:siRNA and L35-PR^+:siRNA, respectively, similar to that reported for lipid-siRNA lipoplexes with a lamellar structure [44]. This feature arises from the fact that the thicknesses of the PR^+ monolayer are all identical and match the HPβCD-$DMEDA^+$ dimensions as described above. If a value of $d_m \approx 4.8$ nm is used for the PR^+ layer thickness, the siRNA monolayer thickness is calculated as $d_w = 3.2 \pm 0.2$ nm. This value is independent of the ρ_{eff} used and is consistent with the presence of a monolayer of hydrated siRNA helixes. Since the detection of a lamellar structure by SAXS, with d and d_w values that are in reasonable agreement with those obtained from cryo-TEM experiments, we conclude that PR^+:siRNA complexes are best characterized as multilamellar structures above the point of electroneutrality (Figure 3C)[45]. The d value estimated by cryo-TEM is approximately 8% lower than the value of d_{100} (~8.0 nm) calculated from the SAXS diffractograms for the L structure of PR^+:siRNA complexes, although the SAXS results are expected to be much more precise in this respect. The clear peak appearing in all diffractograms at higher q factors that is not associated with the lamellar structure is related to the intralayer siRNA - siRNA separation (d_{siRNA}), as previously reported previously by Safinya and co-workers [46, 47]. This feature ($q_{siRNA} = 2\pi/d_{siRNA}$) enables the determination of the separation between siRNA strands within the siRNA monolayer (d_{siRNA}) as $d_{siRNA} = 2.3 – 3.2$ nm for the PR^+:siRNA complexes (Table S-1), that is slightly lower than those reported for lipoplexes studies [31, 38, 46]. The lower d_{siRNA} value obtained for the PR^+:siRNA complexes may be attributed to the fact that, in the mixed lipid compositions used in most lipoplex formulations, the cationic lipid molecules are phase-separated within the bilayer and concentrated near the nucleic acid chains and separated by domains of helper lipid (e.g., neutral or zwitterionic components of the lipid mixture)[48–50], whereas in these PR^+: siRNA complexes, the positive charges of the PR^+ component are more closely and evenly spaced, thus, leading to a reduction in the siRNA-siRNA separation.

Cytotoxicity and RNAi Evaluation

The cell viability of PR^+:siRNA complexes were evaluated in HeLa-GFP and NIH 3T3-GFP cells as a function of ρ_{eff} ratio (Figure 4A) to compare the cytotoxicity profile of the various transfection agents as a function of their charge densities and molecular weight. The toxicity profile were also compared with L2K, a commercial transfection agent which was used as the benchmark for these experiments.

The relative cell viability profiles of the PR^+:siRNA and L2K:siRNA complexes were evaluated by MTS assay. In HeLa-GFP cells, all the PR^+ had cell viability profiles that were comparable or better than L2K, with L81-PR^+ showing the best cell viability (>90%). For all the PR^+:siRNA, increasing ρ_{eff} caused increased cytotoxicity; however, cytotoxicity at the highest concentrations of PR^+ (ρ_{eff}= 15) were modest, affecting only 10 – 20% of the total cell population. Since L81-PR^+ has the highest charge density, a smaller quantity of this PR^+ was required to achieve a target ρ_{eff} upon siRNA complexation compared to the amounts required to achieve the same ρ_{eff} with L35-PR^+ and F127-PR^+. A similar trend in cytotoxicity was also observed in NIH 3T3-GFP cells (Figure S-4). We conclude that the L81-PR^+ complexes are less cytotoxic, since they require lower concentration of cationic polymer to produce effective transfection complexes [51].

The *in vitro* cellular localization profiles of PR^+:siRNA-Cy3 complexes were assessed in HeLa-GFP cells at various ρ_{eff} ratios in serum free media (Figure 4B) under conditions that were optimized for L2K:siRNA complexes. It was observed that L2K complexes had cellular localization profile of ~80%, as reported previously [33].

L81-PR^+:siRNA and L35-PR^+:siRNA complexes had comparable or better cellular uptake efficiencies (≥ 90%) relative to L2K at ρ_{eff} ratios above 1.5; however, the uptake levels of F127-PR^+:siRNA complexes was slightly lower than the rest PR^+ members of the family at all ρ_{eff} ratios studied. In all cases, the uptake efficiency increased with increasing ρ_{eff} until reaching a plateau near ρ_{eff}= 10. It is interesting to note that increased localization correlated with increased positive ζ (e.g., for L81-PR^+:siRNA, there is a significant increase in localization from ρ_{eff} =1.5 to 5; however, after ρ_{eff} = 5, very modest increases were observed). Similar behavior was noted for L35-PR^+:siRNA and F127-PR^+:siRNA at ρ_{eff} =10. We attribute the high localization efficiency of L81-PR^+:siRNA to the enhanced stability of these complexes in the presence of biogenic polyanions present under cell culture conditions, thereby leading to higher cellular association. Moreover, better complexation also contributes to higher cargo loading, making each endocytic event more productive with respect to siRNA uptake. In summary, all of the PR^+ family members could promote the siRNA uptake in 80 – 98% of the total cell population.

The gene silencing efficiency of the PR^+:siRNA complexes was assessed in HeLa-GFP and NIH 3T3-GFP cells using a two-color flow cytometry assay. The RNAi experiment was run in tandem with a cell viability assay to enable the measurement of both these parameters in the same experiment. The experiment was performed with untreated cells and cell treated with PR^+: scrambled RNA (NC-RNA) as a negative control and L2K as a positive control. The gene silencing efficiency was monitored by observing the percentage of the total cell population that displayed a reduction in GFP expression (Figure 5A), as well as a reduction in median fluorescence efficiency (MFI) (Figure 5B). Cell viability was measured by SYTOX® Red dead staining, which only stains the nucleic acids of membrane-compromised dead and dying cells.

HeLa-GFP experiments revealed that the silencing efficiency was dependent on the ρ_{eff} ratio and the PR^+ family member that was used. We found that at their maximum ρ_{eff} ratio, all PR^+:siRNA complexes had remarkable silencing efficiency. Nonetheless, each PR^+ reached

the maximum silencing efficiency at a different ρ_{eff} that was similar to the ρ_{eff} observed to produce a plateau in cellular localization (Figure 4B) and the zeta potential plot (Figure 2). Very similar observations were made for NIH 3T3-GFP cells, where all the PR^+ displayed the same trend of increased silencing efficiency with increased ρ_{eff} up to the plateau level; however, in this cell line, the silencing was not as robust as for L2K (Figure S-6). The comparison between the silencing efficiency of NC-siRNA and untreated cells results were significant ($p < 0.05$), which could be due to the moderate toxicity as evidenced by the cell viability values on Y2 axis on Figure 5b.

Cell viabilities, measured in tandem with silencing efficiencies using SYTOX® Red dead stain to label the membrane-compromised cells, showed that cells treated with the PR^+ complexes had viabilities between 80% - 90%, regardless of the PR^+ used, although the cell viability dropped from 90%) to 80% when the ρ_{eff} ratio approached the plateau level. These cell viability profiles were similar to the commercial reagent, L2K, used as a standard in these experiments. The comparison between untreated and PR^+:siRNA treated results at all p_{eff} ratio (except $p_{eff}{}^{=}$ 1.5) was significant (was <0.01, n=6)

Intracellular Trafficking of PR^+:pDNA Complexes

Cellular uptake and intracellular trafficking of siRNA complexes formed with L81-PR^+:siRNA was studied as a function of time by confocal microscopy (Figure 6). It was observed 2 h after treatment with transfection complexes that few particles were associated with the cells; however, the L81-PR^+:siRNA complex binding and internalization increased significantly between 2 – 4 h incubation, such that a large population of transfection complexes (green) were seen in association with cell membranes (blue), accompanied by a smaller number that were associated with acidic endosomal and lysosomal compartments (red). Moreover, the z-stack images of individual cells at each time point indicate that most of the particles are only at the surface of the cell after 2h, while at 4h, many particles have been internalized. As the time after exposure increased, most of the particles appeared to be interacting with acidic endosomes and lysosomes, depicted as yellow fluorescence in the images due to overlap of the red LysoTracker® and green PR^+:siRNA-Cy3 signals (Figure 7). Interestingly, with increasing time, the green signal due to the transfection complexes seems to fade gradually, likely due to escape of siRNA from the nanocomplexes and distribution throughout the cytoplasm, causing a diminution of the signal below detectable levels (Figure 8). Cells treated with L81-PR^+:siRNA complexes were compared to untreated cells with respect to dynamic expression of GFP. It was found that the MFI in untreated cells remained consistent throughout the incubation, while in the case of L81-PR^+:siRNA-treated cells, the MFI gradually decreased up to 40% rfu relative to controls at 36 h. Most of the cells showed almost no signal, while a few showed a significantly reduced GFP fluorescence (Figure S-7). The reduction in MFI can be directly correlated with the silencing effect and is consistent with the quantitative data obtained from flow cytometry.

Structure-Knockdown Activity Relationship

When siRNA is initially compacted by the PR^+, it is expected that the resulting structure will depend on the magnitude of the intermolecular interactions and the conformational dynamics of the two polyions, PR^+ and siRNA. It is also anticipated that the polyplex

structure (inverted hexagonal, lamellar or cubic) would influence its silencing efficiency upon contact and internalization by the cells. In fact, systematic studies of the structure and knockdown efficiency of lipoplexes containing different cationic lipids have made it possible to establish a correlation between the coexistence of several lipoplex structures and higher transfection efficiency. [38, 44] Those results suggest that knockdown is synergized by the presence of structural polymorphism. As the results above show, SAXS and cryo-TEM experiments indicate that only one lamellar structure is present in the transfection complexes. Thus, there must be other effects to explain why the knockdown efficiency follows the trend L81-PR^+:siRNA > L35-PR^+:siRNA > F127-PR^+:siRNA.

In this sense, the slope of the ζ-potential sigmoidal plots (Figure 2) may be used as an indication of the relative strength of electrostatic interactions between the PR^+ and siRNA cargo. Based on that, the L81-PR^+:siRNA complex showed the highest slope (7 mV/mass), L35-PR^+:siRNA complex showed an intermediate slope (1 mV/mass) while the F127-PR^+:siRNA complex showed the most smoothed slope (0.35 mV/mass), thus suggesting a trend of decreasing electrostatic interactions in this respective order. In addition, DLS, gel shift (Figure S1–S3), cryo-TEM, and SAXS (Figure 3) results obtained for all the polyplexes confirms the trend of a gradual increase in electrostatic interaction between siRNA and F127-, L35- and L81-based PR^+, respectively. These differences in electrostatic interactions between PR^+ and siRNA are rooted in the structural differences of the PR^+ at the molecular level. Based on previous literature of Pluronic®-derived PR^+, the CDs are localized predominantly on the PO block rather than the EO block. Moreover, it has been shown that each CD includes two PO monomer units [52].

Other studies have also shown that higher CD threading restricts the flexibility of the polymer and forms a rigid rod like structure[25, 53], thus we believe that threading not only increases the probability for siRNA interactions via encounter of two rod-like objects, but also helps maintain the relative stoichiometry balance (i.e. effective charges) between the PR^+ cations and the siRNA anions. This hypothesis is supported by our cryo-TEM observations (Figure 3A) showing that the fingerprint multilamellar pattern of the L81-PR^+: siRNA complexes is more structured, with large nano-aggregates containing more multilayers and a clear spherical morphology, than for the L35-PR^+: siRNA complexes. The observations made on the basis of biological data for the PR^+ family suggests that the transfection efficiency is in the decreasing order as L81-PR^+:siRNA> L35-PR^+:siRNA> F127-PR^+:siRNA. Although there can be many parameters such as difference in hydrophobicity of the polymers, complex structures, electrostatic interaction or rigidity that could impact their relative transfection efficiencies, based on our observation of SAXS and cryo-TEM data, we believe that the rigid structure resulting from the most ordered complexes is the main factor that promotes the highest transfection activity. Our findings show that F127-PR^+ has the lowest threading efficiency (~30%), compared to L35- (88%) and L81-PR^+ (56%), as well as the longest EO length. These factors combine to hinder the formation of strong network of electrostatic interactions between F127-$PR^+$and siRNA (Figure 9). These weaker interactions may be responsible for the lower silencing efficiency compared to the other members of the PR^+ family due to colloidal instability under cell culture conditions such that uptake of siRNA complexes is less effective for F127-PR^+. Between the highly threaded members (L35-PR^+ and L81-PR^+), L35 has the higher HPβCD

threading efficiency, thereby increasing the probability of strong electrostatic interactions with siRNA; however, the longer EO blocks of L35 may partially disrupt its interactions with the siRNA cargo. Consequently, the L35-PR^+:siRNA complexes possess weaker electrostatic interactions than L81-PR^+, which has lower threading but a very short EO chain, leading to the production of complexes with greater colloidal stability, cellular uptake, and knockdown efficiency. We conclude the silencing efficiency of PR^+:siRNA complexes is most highly dependent on strong electrostatic interaction between the PR^+ condensing agent and siRNA, with the formation of a highly ordered lamellar architecture of the complex as a factor of secondary importance. The electrostatic interaction dependence of these two key parameters, i.e., threading efficiency and the length of the EO block, to produce a lamellar architecture is a direct result of the increased rigidity of the threaded PR^+ [54–56].

CONCLUSIONS

Three novel Pluronic®-based, cholesterol end-capped cationic polyrotaxanes bearing DMEDA-modified 2-hydroxypropyl-β-cyclodextrin macrocycles were synthesized and evaluated for their siRNA delivery efficiency. Cytotoxicity experiments show that the PR^+:siRNA complexes are well tolerated. RNAi experiments indicate that they are capable of efficient silencing (>80%) in multiple cell lines in a manner that is influenced by the effective charge ratio (ρ_{eff}), PO block length, and central block coverage (i.e., rigidity) of the PR^+ core. DLS measurements show that particles in the 200 – 300 nm range are formed by the PR^+:siRNA complexes. SAXS and cryo-TEM experiments studies reveal that these particles are comprised of periodic, lamellar architectures. These findings suggest that compact PR^+:siRNA nanostructures can produced having higher transfection performance than Lipofectamine® 2000 in cell line such as HeLa and NIH 3T3 *in vitro*, while maintaining good cell viability and siRNA sequence protection in cell culture. We further conclude that knockdown efficiency by PR^+:siRNA complexes is most highly dependent on strong electrostatic interaction between the PR^+ condensing agent and siRNA, with the formation of a highly ordered lamellar architecture of the complex as a secondary factor. The electrostatic interaction is dependent on two key parameters i.e higher threading efficiency and the shorter length of the non-cationic part of polymer (i.e. EO domain), which are also responsible for the increased rigidity of the threaded PR^+.

Supplementary Material

Refer to Web version on PubMed Central for supplementary material.

Acknowledgments

The authors gratefully acknowledge the support of NIH RO1 GM087016 and R21 CA15196. The NMR, MS and flow cytometry data were acquired using facilities grant to Purdue University of Center for Cancer Research supported by the P30 CA023168. Professor Emilio Aicart thanks the MEC of Spain for supporting his stay at Purdue University under the Program “Salvador de Madariaga”. The assistance of Dr. Aaron Taylor with the confocal microscopy experiments, Dr. Jeffrey Woodliff with flow cytometry experiments, and Professor Horia Petrache with small angle x-ray scattering experiments is also gratefully acknowledged.

Abbreviation

PO	polypropylene alcohol
EO	polyethylene alcohol
HPβCD	2-Hydroxypropyl-β-cyclodextrin
PR$^+$	cationic polyrotaxanes
L2K	Lipofectamine® 2000

References

1. Resnier P, Montier T, Mathieu V, Benoit JP, Passirani C. A review of the current status of sirna nanomedicines in the treatment of cancer. Biomaterials. 2013; 34:6429–6443. [PubMed: 23727262]
2. Kanasty R, Dorkin JR, Vegas A, Anderson D. Delivery materials for sirna therapeutics. Nat Mater. 2013; 12:967–977. [PubMed: 24150415]
3. Breunig M, Lungwitz U, Liebl R, Goepferich A. Breaking up the correlation between efficacy and toxicity for nonviral gene delivery. P Natl Acad Sci USA. 2007; 104:14454–14459.
4. Wan C, Allen TM, Cullis PR. Lipid nanoparticle delivery systems for sirna-based therapeutics. Drug Deliv Transl Re. 2014; 4:74–83.
5. Chaturvedi K, Ganguly K, Kulkarni AR, Kulkarni VH, Nadagouda MN, Rudzinski WE, et al. Cyclodextrin-based sirna delivery nanocarriers: A state-of-the-art review. Expert Opin Drug Del. 2011; 8:1455–1468.
6. Li J, Chen YC, Tseng YC, Mozumdar S, Huang L. Biodegradable calcium phosphate nanoparticle with lipid coating for systemic sirna delivery. J Control Release. 2010; 142:416–421. [PubMed: 19919845]
7. Lee SK, Han MS, Asokan S, Tung CH. Effective gene silencing by multilayered sirna-coated gold nanoparticles. Small. 2011; 7:364–370. [PubMed: 21294265]
8. Shi JJ, Xiao ZY, Votruba AR, Vilos C, Farokhzad OC. Differentially charged hollow core/shell lipid-polymer-lipid hybrid nanoparticles for small interfering rna delivery. Angew Chem Int Edit. 2011; 50:7027–7031.
9. Draz MS, Fang BA, Zhang PF, Hu Z, Gu SD, Weng KC, et al. Nanoparticle-mediated systemic delivery of sirna for treatment of cancers and viral infections. Theranostics. 2014; 4:872–892. [PubMed: 25057313]
10. Kanasty RL, Whitehead KA, Vegas AJ, Anderson DG. Action and reaction: The biological response to sirna and its delivery vehicles. Mol Ther. 2012; 20:513–524. [PubMed: 22252451]
11. Landesman-Milo D, Peer D. Toxicity profiling of several common rnai-based nanomedicines: A comparative study. Drug Deliv Transl Res. 2014; 4:96–103. [PubMed: 25786620]
12. Borna H, Imani S, Iman M, Azimzadeh Jamalkandi S. Therapeutic face of rnai: In vivo challenges. Expert opinion on biological therapy. 2015; 15:269–285. [PubMed: 25399911]
13. Zeng H, Johnson ME, Oldenhuis NJ, Tiambeng TN, Guan Z. Structure-based design of dendritic peptide bolaamphiphiles for sirna delivery. ACS Cent Sci. 2015; 1:303–312. [PubMed: 26436138]
14. Aliabadi HM, Landry B, Sun C, Tang T, Uludağ H. Supramolecular assemblies in functional sirna delivery: Where do we stand? Biomaterials. 2012; 33:2546–2569. [PubMed: 22209641]
15. Yang C, Wang X, Li HZ, Goh SH, Li J. Synthesis and characterization of polyrotaxanes consisting of cationic alpha-cyclodextrins threaded on poly[(ethylene oxide)-ran-(propylene oxide)] as gene carriers. Biomacromolecules. 2007; 8:3365–3374. [PubMed: 17929967]
16. Ooya T, Choi HS, Yamashita A, Yui N, Sugaya Y, Kano A, et al. Biocleavable polyrotaxane - plasmid DNA polyplex for enhanced gene delivery. J Am Chem Soc. 2006; 128:3852–3853. [PubMed: 16551060]

17. Yamada Y, Nomura T, Harashima H, Yamashita A, Yui N. Post-nuclear gene delivery events for transgene expression by biocleavable polyrotaxanes. Biomaterials. 2012; 33:3952–3958. [PubMed: 22386920]
18. Yamashita A, Kanda D, Katoono R, Yui N, Ooya T, Maruyama A, et al. Supramolecular control of polyplex dissociation and cell transfection: Efficacy of amino groups and threading cyclodextrins in biocleavable polyrotaxanes. J Controlled Release. 2008; 131:137–144.
19. Zhou Y, Wang H, Wang CX, Li YS, Lu WF, Chen SF, et al. Receptor-mediated, tumor-targeted gene delivery using folate-terminated polyrotaxanes. Molecular Pharmaceutics. 2012; 9:1067–1076. [PubMed: 22482910]
20. Dandekar P, Jain R, Keil M, Loretz B, Muijs L, Schneider M, et al. Cellular delivery of polynucleotides by cationic cyclodextrin polyrotaxanes. J Controlled Release. 2012; 164:387–393.
21. Kulkarni A, DeFrees K, Schuldt RA, Hyun SH, Wright KJ, Yerneni CK, et al. Cationic alpha-cyclodextrin:Poly(ethylene glycol) polyrotaxanes for sirna delivery. Molecular Pharmaceutics. 2013; 10:1299–1305. [PubMed: 23398604]
22. Kulkarni A, DeFrees K, Schuldt RA, Vlahu A, VerHeul R, Hyun SH, et al. Multi-armed cationic cyclodextrin:Poly(ethylene glycol) polyrotaxanes as efficient gene silencing vectors. Integr Biol-Uk. 2013; 5:115–121.
23. Tamura A, Yui N. Cellular internalization and gene silencing of sirna polyplexes by cytocleavable cationic polyrotaxanes with tailored rigid backbones. Biomaterials. 2013; 34:2480–2491. [PubMed: 23332177]
24. Utsunomiya H, Katoono R, Yui N, Sugiura T, Kubo Y, Kato Y, et al. Cationic polyrotaxanes effectively inhibit uptake via carnitine/organic cationic transporters without cytotoxicity. Macromol Biosci. 2008; 8:665–669. [PubMed: 18366149]
25. Yokoyama N, Seo JH, Tamura A, Sasaki Y, Yui N. Tailoring the supramolecular structure of aminated polyrotaxanes toward enhanced cellular internalization. Macromol Biosci. 2014; 14:359–368. [PubMed: 24634263]
26. Gould S, Scott RC. 2-hydroxypropyl-beta-cyclodextrin (hp-beta-cd): A toxicology review. Food Chem Toxicol. 2005; 43:1451–1459. [PubMed: 16018907]
27. Badwaik V, Mondjinou Y, Kulkarni A, Liu L, Demoret A, Thompson DH. Efficient pdna delivery using cationic 2-hydroxypropyl-beta-cyclodextrin pluronic-based polyrotaxanes. Macromol Biosci. 2015
28. Mondjinou YA, McCauliff LA, Kulkarni A, Paul L, Hyun SH, Zhang Z, et al. Synthesis of 2-hydroxypropyl-beta-cyclodextrin/pluronic-based polyrotaxanes via heterogeneous reaction as potential niemann-pick type c therapeutics. Biomacromolecules. 2013; 14:4189–4197. [PubMed: 24180231]
29. Bednar J, Woodcock CL. Cryoelectron microscopic analysis of nucleosomes and chromatin. Methods Enzymol. 1999; 304:191–213. [PubMed: 10372361]
30. Dubochet J, Adrian M, Chang JJ, Homo JC, Lepault J, McDowall AW, et al. Cryo-electron microscopy of vitrified specimens. Quarterly reviews of biophysics. 1988; 21:129–228. [PubMed: 3043536]
31. Misra SK, Munoz-Ubeda M, Datta S, Barran-Berdon AL, Aicart-Ramos C, Castro-Hartmann P, et al. Effects of a delocalizable cation on the headgroup of gemini lipids on the lipoplex-type nanoaggregates directly formed from plasmid DNA. Biomacromolecules. 2013; 14:3951–3963. [PubMed: 24083552]
32. Barran-Berdon AL, Misra SK, Datta S, Munoz-Ubeda M, Kondaiah P, Junquera E, et al. Cationic gemini lipids containing polyoxyethylene spacers as improved transfecting agents of plasmid DNA in cancer cells. J Mater Chem B. 2014; 2:4640–4652.
33. Amenitsch H, Caracciolo G, Foglia P, Fuscoletti V, Giansanti P, Marianecci C, et al. Existence of hybrid structures in cationic liposome/DNA complexes revealed by their interaction with plasma proteins. Colloid Surface B. 2011; 82:141–146.
34. Ewert KK, Evans HM, Bouxsein NF, Safinya CR. Dendritic cationic lipids with highly charged headgroups for efficient gene delivery. Bioconjugate Chem. 2006; 17:877–888.

35. Rodriguez-Pulido A, Aicart E, Junquera E. Electrochemical and spectroscopic study of octadecyltrimethylammonium bromide/DNA surfoplexes. Langmuir. 2009; 25:4402–4411. [PubMed: 19366220]
36. Pereira P, Jorge AF, Martins R, Pais AACC, Sousa F, Figueiras A. Characterization of polyplexes involving small rna. J Colloid Interface Sci. 2012; 387:84–94. [PubMed: 22980740]
37. Munoz-Ubeda M, Misra SK, Barran-Berdon AL, Aicart-Ramos C, Sierra MB, Biswas J, et al. Why is less cationic lipid required to prepare lipoplexes from plasmid DNA than linear DNA in gene therapy? J Am Chem Soc. 2011; 133:18014–18017. [PubMed: 21985329]
38. Munoz-Ubeda M, Misra SK, Barran-Berdon AL, Datta S, Aicart-Ramos C, Castro-Hartmann P, et al. How does the spacer length of cationic gemini lipids influence the lipoplex formation with plasmid DNA? Physicochemical and biochemical characterizations and their relevance in gene therapy. Biomacromolecules. 2012; 13:3926–3937. [PubMed: 23130552]
39. Jensen LB, Mortensen K, Pavan GM, Kasimova MR, Jensen DK, Gadzhyeva V, et al. Molecular characterization of the interaction between sirna and pamam g7 dendrimers by saxs, itc, and molecular dynamics simulations. Biomacromolecules. 2010; 11:3571–3577. [PubMed: 21067145]
40. Jiang RC, Lu XM, Yang MH, Deng WX, Fan QL, Huang W. Monodispersed brush-like conjugated polyelectrolyte nanoparticles with efficient and visualized sirna delivery for gene silencing. Biomacromolecules. 2013; 14:3643–3652. [PubMed: 24040909]
41. Kesharwani P, Gajbhiye V, Jain NK. A review of nanocarriers for the delivery of small interfering rna. Biomaterials. 2012; 33:7138–7150. [PubMed: 22796160]
42. Yue YN, Wu C. Progress and perspectives in developing polymeric vectors for in vitro gene delivery. Biomater Sci-Uk. 2013; 1:152–170.
43. Zhang Y, Chen J, Xiao CS, Li MQ, Tian HY, Chen XS. Cationic dendron-bearing lipids: Investigating structure-activity relationships for small interfering rna delivery. Biomacromolecules. 2013; 14:4289–4300. [PubMed: 24144000]
44. Desigaux L, Sainlos M, Lambert O, Chevre R, Letrou-Bonneval E, Vigneron JP, et al. Self-assembled lamellar complexes of sirna with lipidic aminoglycoside derivatives promote efficient sirna delivery and interference. P Natl Acad Sci USA. 2007; 104:16534–16539.
45. Koltover I, Salditt T, Safinya CR. Phase diagram, stability, and overcharging of lamellar cationic lipid-DNA self-assembled complexes. Biophys J. 1999; 77:915–924. [PubMed: 10423436]
46. Bouxsein NF, McAllister CS, Ewert KK, Samuel CE, Safinya CR. Structure and gene silencing activities of monovalent and pentavalent cationic lipid vectors complexed with sirna. Biochemistry-Us. 2007; 46:4785–4792.
47. Leal C, Bouxsein NF, Ewert KK, Safinya CR. Highly efficient gene silencing activity of sirna embedded in a nanostructured gyroid cubic lipid matrix. J Am Chem Soc. 2010; 132:16841–16847. [PubMed: 21028803]
48. Caracciolo G, Pozzi D, Amici A, Amenitsch H. Universality of DNA adsorption behavior on the cationic membranes of nanolipoplexes. J Phys Chem B. 2010; 114:2028–2032. [PubMed: 20078061]
49. Bouxsein NF, McAllister CS, Ewert KK, Samuel CE, Safinya CR. Structure and gene silencing activities of monovalent and pentavalent cationic lipid vectors complexed with sirna. Biochemistry-Us. 2007; 46:4785–4792.
50. Kumar K, Barran-Berdon AL, Datta S, Munoz-Ubeda M, Aicart-Ramos C, Kondaiah P, et al. A delocalizable cationic headgroup together with an oligo-oxyethylene spacer in gemini cationic lipids improves their biological activity as vectors of plasmid DNA. Journal of Materials Chemistry B. 2015; 3:1495–1506.
51. Carr LR, Jiang S. Mediating high levels of gene transfer without cytotoxicity via hydrolytic cationic ester polymers. Biomaterials. 2010; 31:4186–4193. [PubMed: 20149427]
52. Harada A, Li J, Kamachi M. Preparation and characterization of a polyrotaxane consisting of monodisperse poly(ethylene glycol) and .Alpha.-cyclodextrins. J Am Chem Soc. 1994; 116:3192–3196.
53. Tonelli AE. Restructuring polymers via nanoconfinement and subsequent release. Beilstein J Org Chem. 2012; 8:1318–1332. [PubMed: 23019466]

54. Asayama S, Nohara A, Negishi Y, Kawakami H. Alkylimidazolium end-modified poly(ethylene glycol) to form the mono-ion complex with plasmid DNA for in vivo gene delivery. Biomacromolecules. 2014; 15:997–1001. [PubMed: 24547884]

55. Foldvari M, Badea I, Wettig S, Verrall R, Bagonluri M. Structural characterization of novel gemini non-viral DNA delivery systems for cutaneous gene therapy. J Exp Nanosci. 2006; 1:165–176.

56. Jarroux N, Guegan P, Cheradame H, Auvray L. High conversion synthesis of pyrene end functionalized polyrotaxane based on poly(ethylene oxide) and alpha-cyclodextrins. J Phys Chem B. 2005; 109:23816–23822. [PubMed: 16375366]

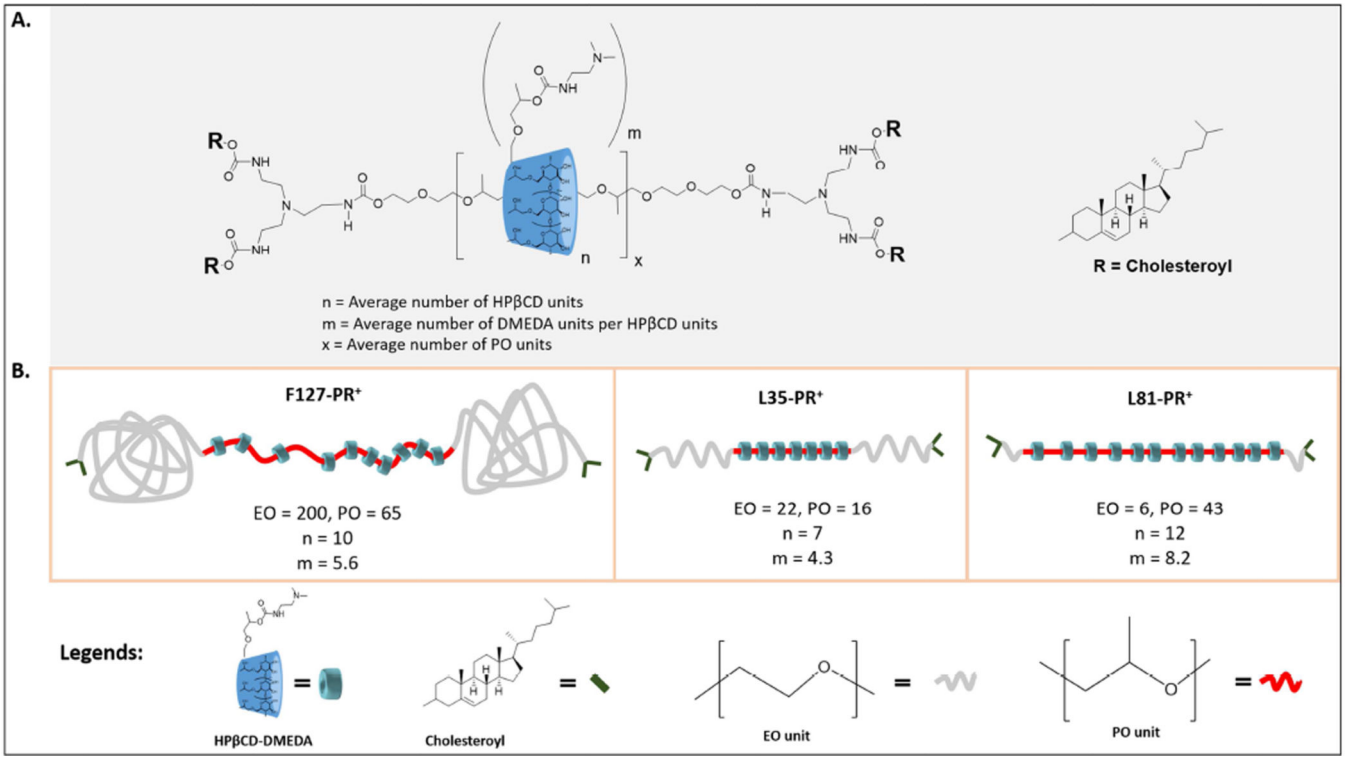

Figure 1.
Chemical structure of DMEDA-HPβCD:Pluronic-Chl Polyrotaxanes (PR^{+}).

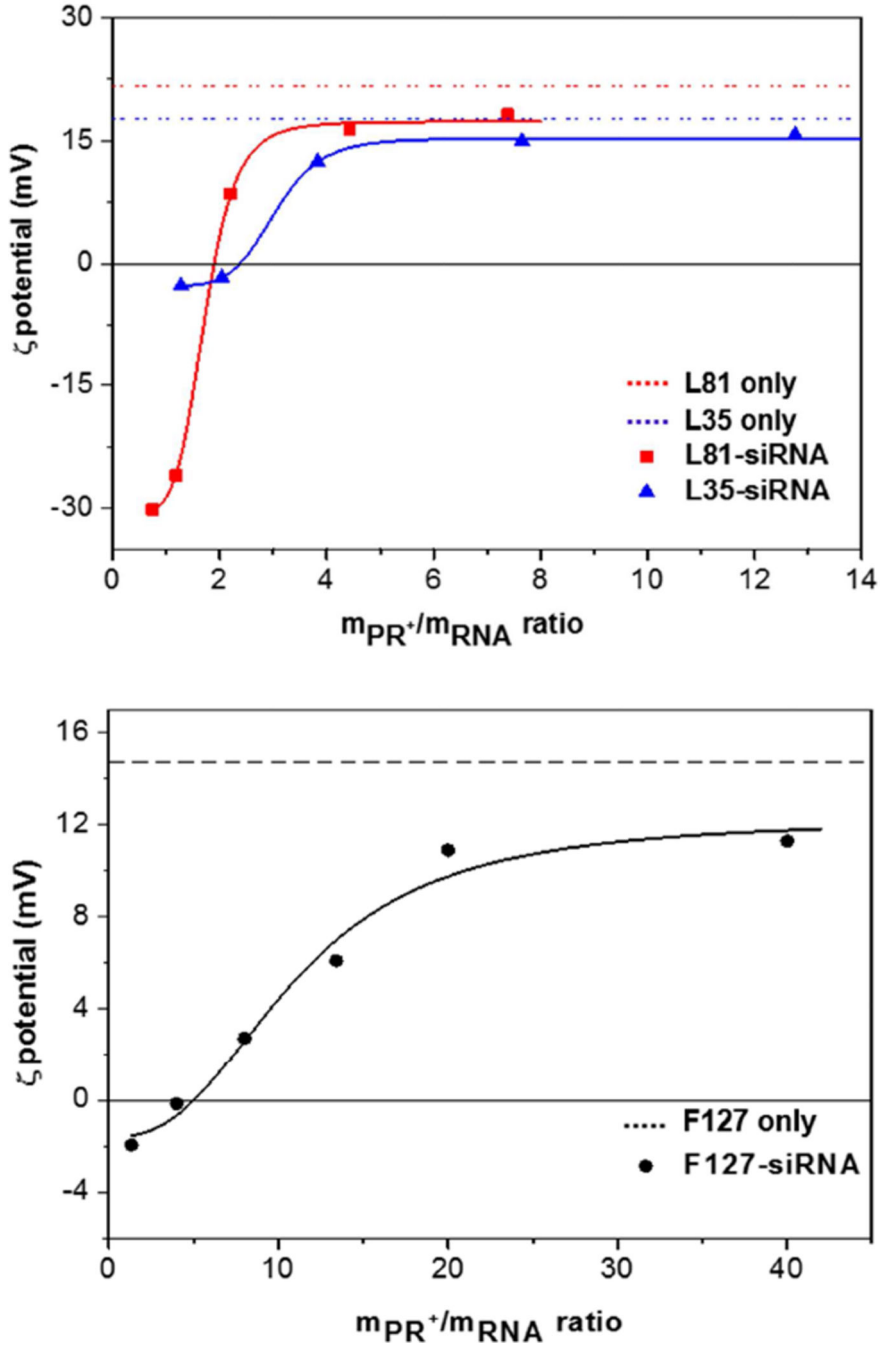

Figure 2.

Dependence of zeta potential (ζ) on polyplex compositions ($m_{PR+/}\ m_{siRNA}$) for L81-PR^+:siRNA, L35-PR^+:siRNA and F127-PR^+:siRNA in HEPES buffer at 20 °C, pH=7.4. The amount of PR^+ was increased relative to siRNA until the formulations showed no significant increase in ζ (plateau phase). The surface charge of PR^+ only (i.e $m_{PR+/}\ m_{SiRNA}= \infty$) is shown by dotted line at the top of each graph, indicating the maximum PR^+ positive surface charge PR^+.

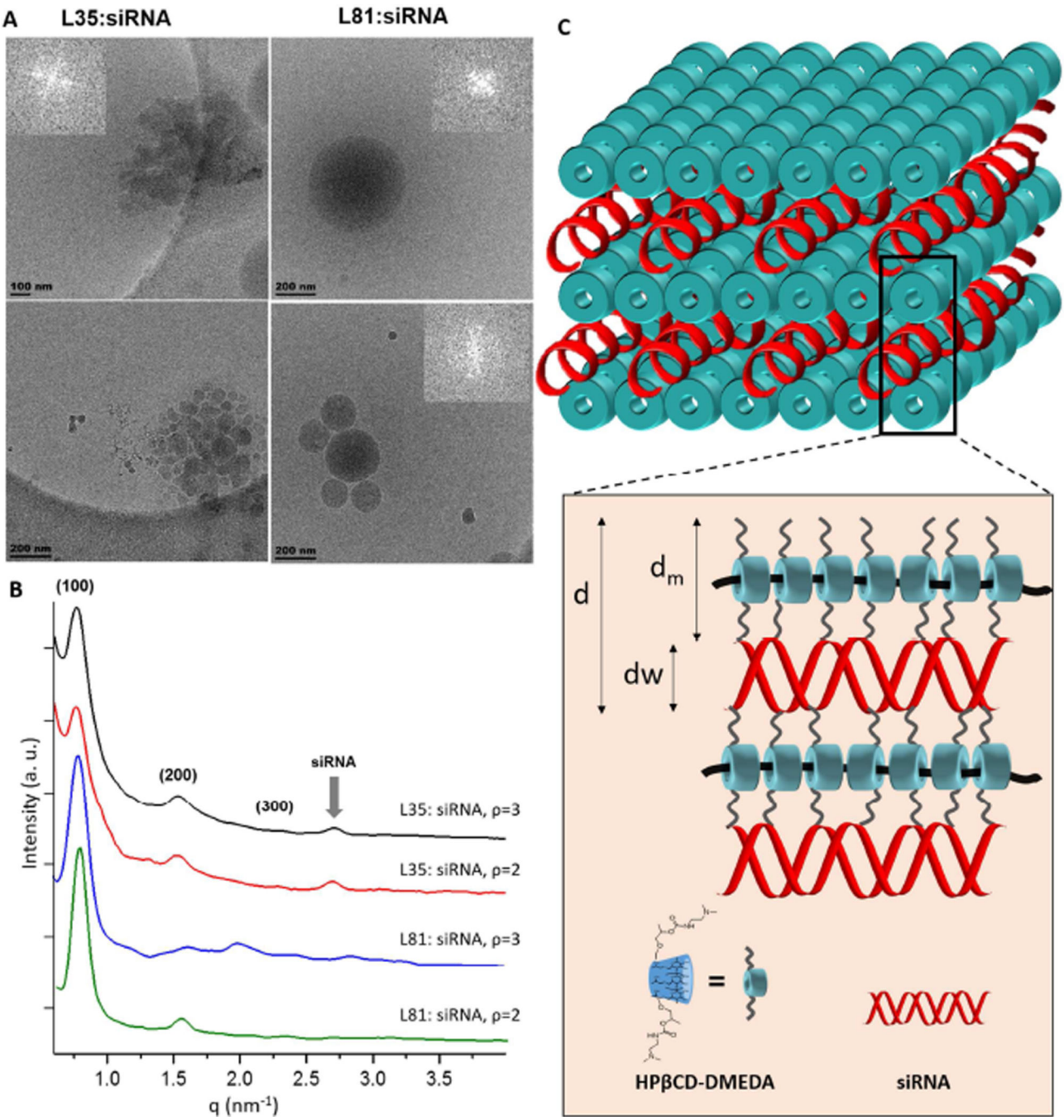

Figure 3.

(A) Selected cryo-TEM micrographs showing a general structure of L35-PR^+:siRNA and L81-PR^+:siRNA at ρ_{eff} = 3. The insets showing a FFT profile from a particular area of the polyplexes. **(B)** SAXS diffractograms of PR^+:siRNA complexes at effective charge ratios of 2 and 3. **(C)** Scheme representing the multilamellar arrangement constituted by a series of PR^+ monolayers with siRNA compacted and sandwiched between them. The interlamellar spacing (d_m) was found to be ~4.8 and thickness of siRNA (d_w) to be ~ 3.2 nm (figure drawn to arbitrary scale)

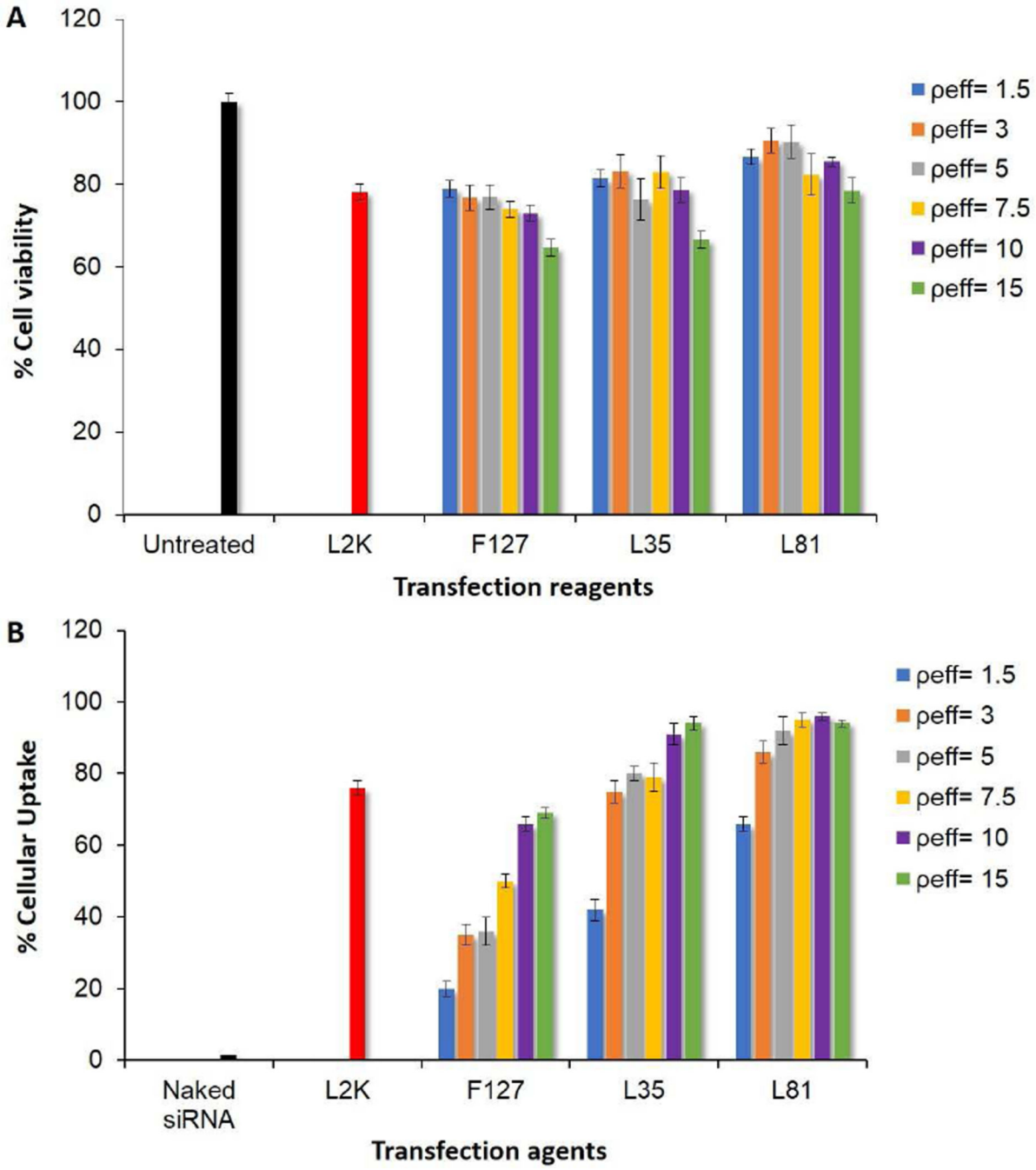

Figure 4.

(A) MTS cell viability assay for HeLa-GFP cells, after 24 h exposure to PR^+:siRNA, L2K:siRNA complexes as function of ρ_{eff} ratios. **(B)** Cell associated fluorescence of naked siRNA, PR^+:siRNA-Cy3(at ρ_{eff} ratios of 1.5 to 15), L2K:siRNA-Cy3 in HeLa-GFP after incubation for 4 h.

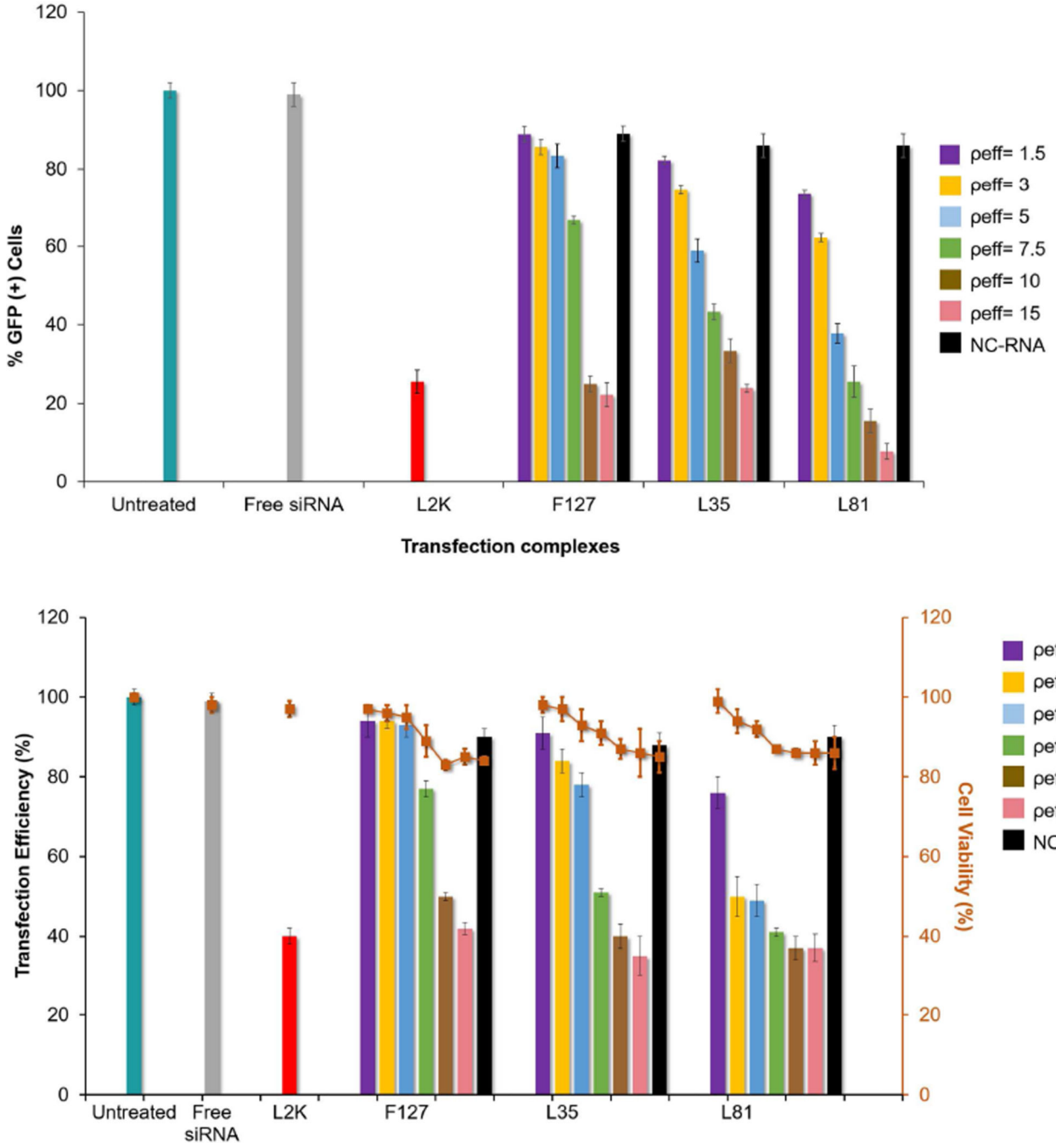

Figure 5.

(A) Flow cytometric analysis of GFP knockdown efficiency (% GFP+ cells) in HeLa-GFP cells after exposure PR^+: siRNA complexes at various ρ_{eff} ratios of 1.5 to 15 with L2K:siRNA as positive controls and untreated cells and cells treated with naked siRNA (free siRNA), PR^+:NC-RNA (scrambled RNA) as negative control. **(B)** Two-color flow-cytometric analysis of GFP knockdown efficiency (median fluorescence intensity) and cyto-toxicity in HeLa-GFP cells after exposure to PR^+:siRNA complexes at various ρ_{eff} ratios of

1.5 to 15 with L2K:siRNA as positive controls and untreated cells, cells treated with naked siRNA (free siRNA and PR^{+}:NC-RNA (scrambled RNA) as negative control.

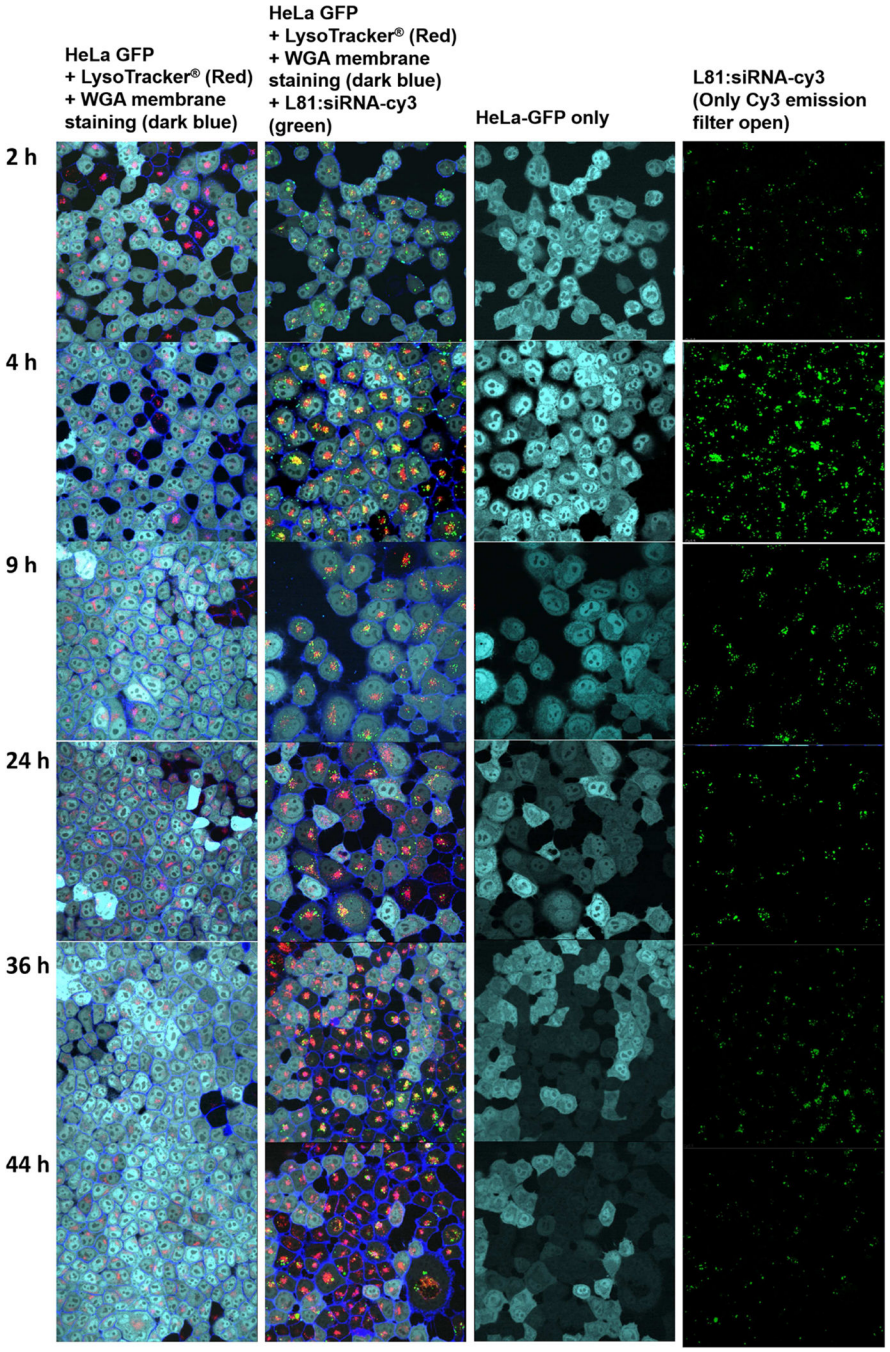

Figure 6.

Multiphoton confocal images of HeLa-GFP cells treated with L81-PR^{+}:siRNA complexes at different time points. Stains: Light blue, stably expressed GFP; Purple, plasma membrane; Red, late endosomes and lysosomes; Green, PR^{+}:siRNA complexes. From top to bottom: Images taken at increasing time points as indicated in front of each row. From left to right: Column 1, LysoTracker® Blue DND-22-stained HeLa-GFP cells (control, untreated with L81-PR^{+}:siRNA complexes); Column 2, HeLa-GFP treated with L81-PR^{+}:siRNA complexes; Column 3, Images from Column 2 in the absence of any stains (GFP

expression); Column 4, Images of Column 2, filtered for fluorescence emission from L81-PR^{+}:siRNA-cy3 complexes only.

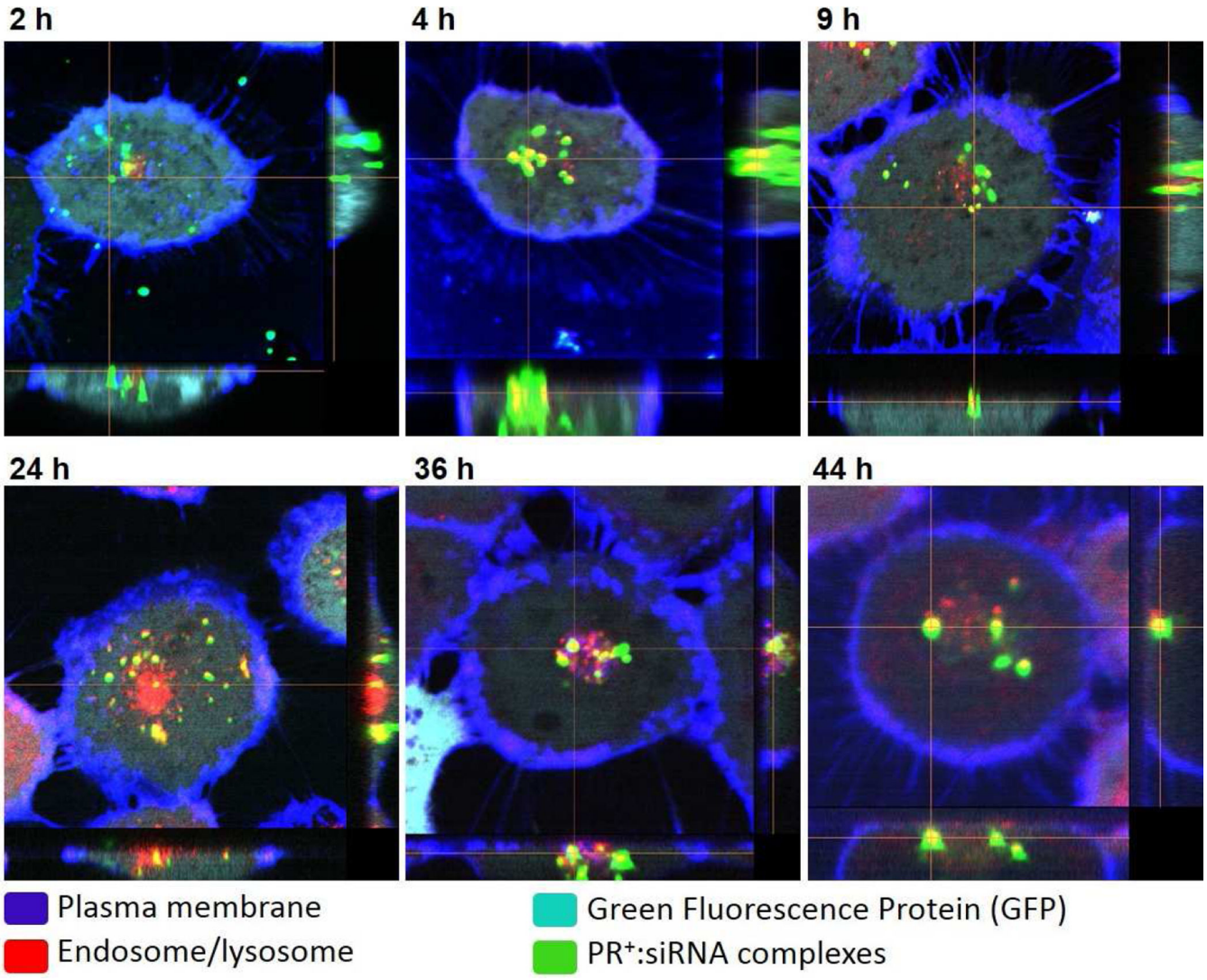

Figure 7.

Z stack images of HeLa-GFP cells treated at different time points, showing the interaction of L81-PR^{+}:siRNA complexes with the acidic compartments after the time point of 2 hrs.

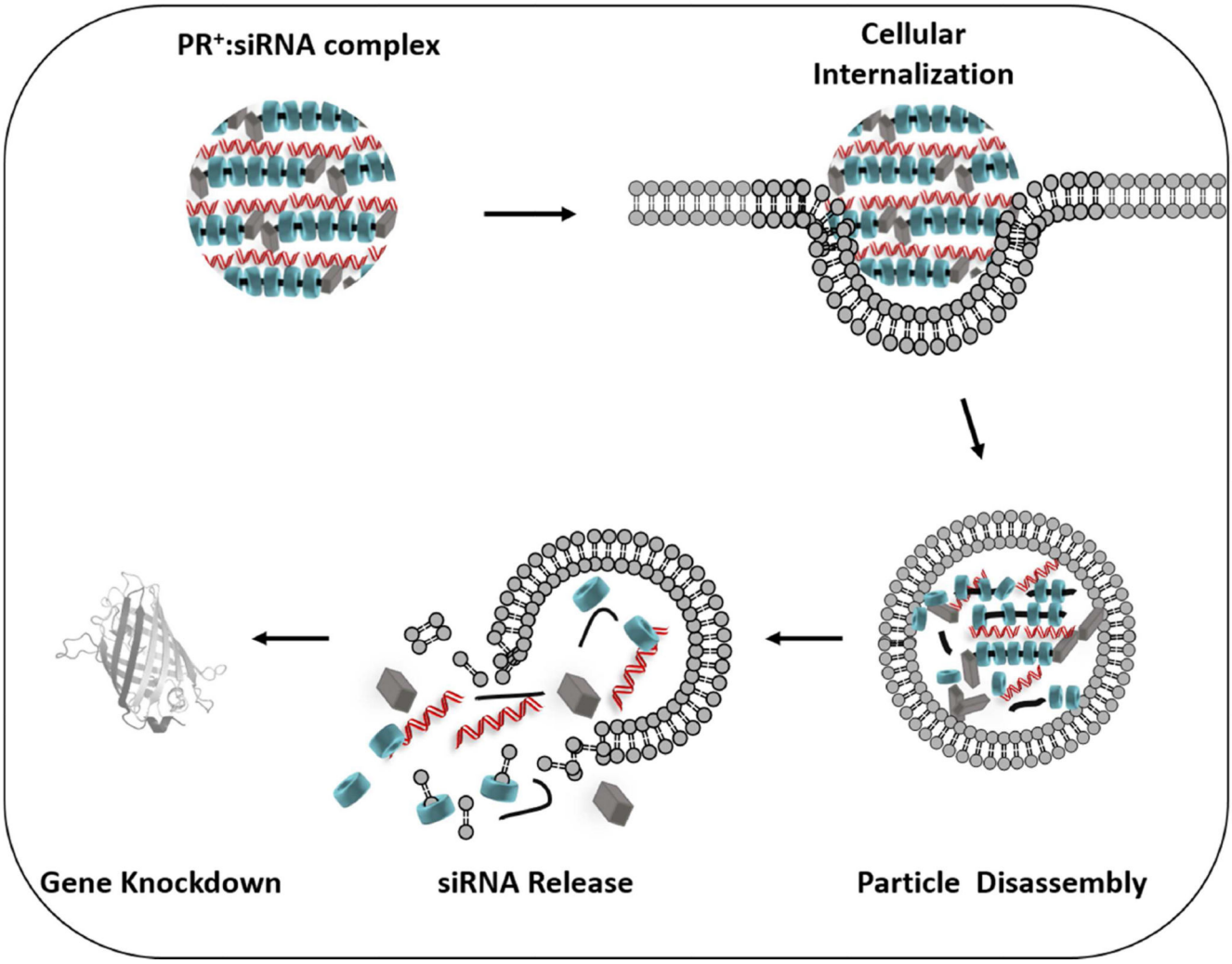

Figure 8.

Conceptual diagram showing PR^+:siRNA complexation, cellular internalization, endocytosis, particle degradation into late endosomal/lysosomal compartments resulting in escape of siRNA from the complexes, and release of siRNA into cytoplasm, to enable gene silencing.

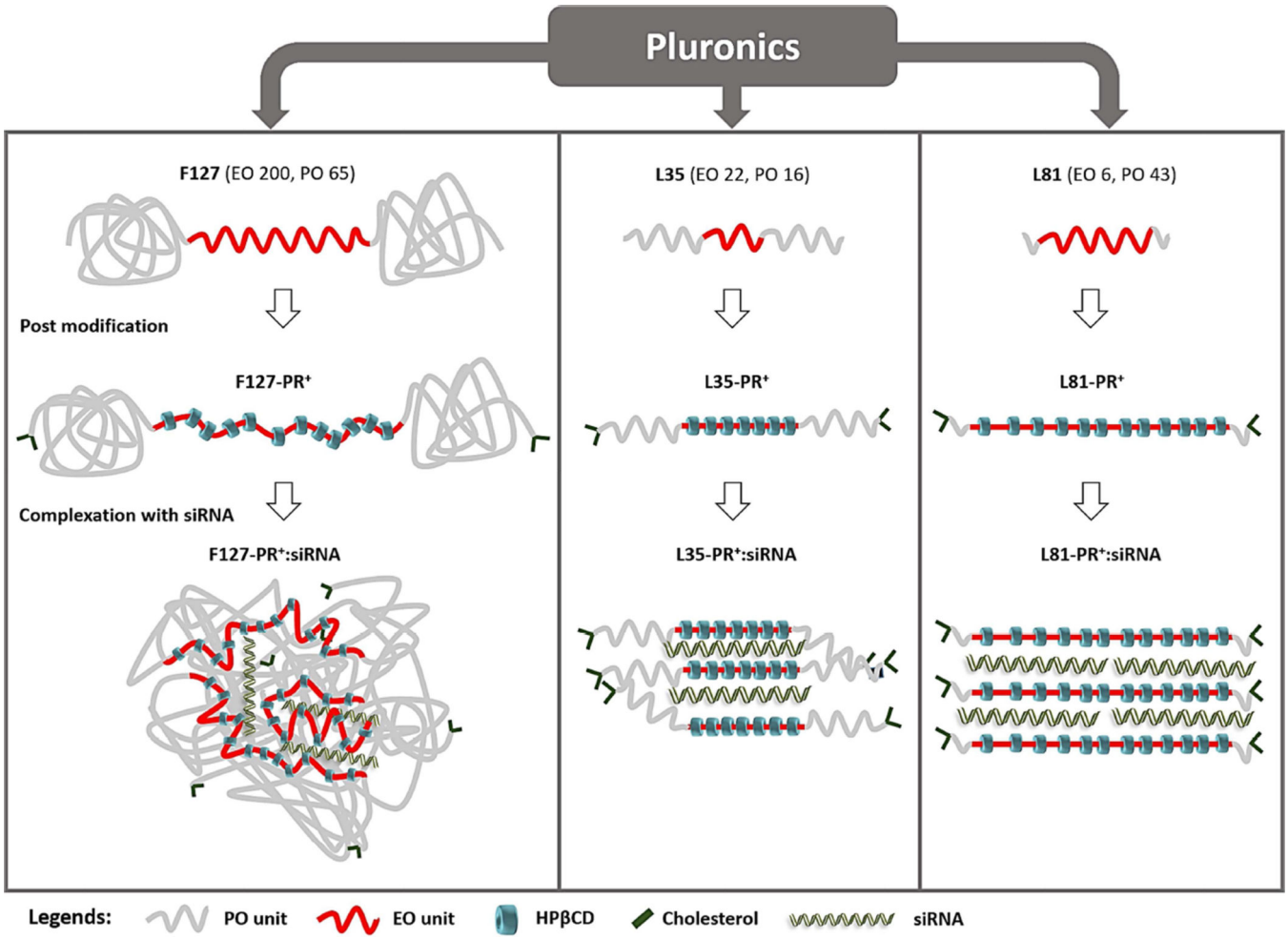

Figure 9.

Representative structures of Pluronic polymers F127, L35 and L81 (Top row) and F127-, L35-, and L81-based polyrotaxanes (middle row) and siRNA:PR^+ complexes (bottom row). The lengths of the polymers and siRNA (22 bp) in these diagrams are approximate and are based on calculations obtained from prior reports [52]. The estimated effective length of the Pluronics and siRNA are as follows F127~87.5 nm (PO~21.5 nm, EO~ 66 nm), L35 ~ 12.5 nm (PO~5.3 nm, EO~ 7.3 nm), L81~ 16.5 nm (PO~14.2 nm, EO~ 2 nm) and siRNA (22 bp) ~7.5 nm[52]. The scheme represents the composition of unmodified polymers that were chosen for PR^+ family based on the total length and distribution of hydrophilic (EO) and hydrophobic (PO) domains. The PR^+ representation shows the variation in threading efficiency, expected structural behaviour of PR^+, and the most probable region of HPβCD localization. Based on previous literature and the data obtained for PR^+:siRNA complexes, it can be concluded that high threading leads to lower flexibility of the PR^+, thus increasing the overall rigidity of the PR^+, such that its rod-like structure helps promote electrostatic interaction with siRNA.

Table 1

Values of the Characteristic Parameters for Polyrotaxanes (PR^+) and Effective Charge, q_{PR^+}, for PR^+-siRNA[a] Polyplex Formulations.

Polyrotaxanes Components	**HPβCD-Chl:Pluronic Polyrotaxanes**		
	L81-PR$^+$	**L35-PR$^+$**	**F127-PR$^+$**
Pluronic® core	L81	L35	F127
Number of HPβCD unis	12	7	10
PR^+ threading efficiency	56%	88%	30%
PR^+ molecular weight	34.4 kD	18.2 kD	35.6 kD
# DMEDA/PR^+ (nominal charge)	98	30	56
q_{PR^+} (effective charge)	57	24	23
% of PR^+ charge available	58	80	41

[a] siRNA used in this work, with a molecular weight of 14.0 kD contains (20+2 ends) bp and thus, $q_{\text{eff RNA}} = q_{\text{nominal RNA}} = 44$.